International Journal of Heat and Technology
Vol. 43, No. 2, April, 2025, pp. 391-402
Journal homepage: http://iieta.org/journals/ijht

Numerical Analysis of Lithium-Ion Electric Vehicle Battery Cooling Efficiency: Evaluating Material Influence on Thermal Performance

Noor H. Jawad[1*], Rawad Luay Abdul Jabbar[2], Karar Saeed Mohammed[3], Muhammad Asmail Eleiwi[4], Hasan Shakir Majdi[5]

[1] Chemical Engineering Department, University of Technology- Iraq, Baghdad 10066, Iraq
[2] Department of Refrigeration and Air Conditioning Technology Engineering, Al-Farahidi University, Baghdad 10017, Iraq
[3] Department of Medical Physics, Almanara College for Medical Sciences, Maysan 62011, Iraq
[4] Electromechanical Engineering Department, College of Engineering, University of Samarra, Samarra 34010, Iraq
[5] Department of Chemical Engineering and Petroleum Industries, Al-Mustaqbal University College, Hillah 51001, Iraq

Corresponding Author Email: noor.h.jawad@uotechnology.edu.iq

https://doi.org/10.18280/ijht.430202

Received: 5 February 2025
Revised: 24 March 2025
Accepted: 9 April 2025
Available online: 30 April 2025

Keywords:
lithium-ion batteries (LIBs), battery thermal management system (BTMS), outer case material selection, cooling system efficiency, ANSYS fluent simulation

ABSTRACT

The researchers performed an investigation to examine how external casing materials affect lithium-ion battery (LIB) thermal behavior within electric vehicles (EVs) for safety improvement and temperature control and operational optimization. The CFD simulations built inside ANSYS Fluent 2022 R2 tested battery thermal functions by studying Al and Cu combined with PVC outer shell designs which served as cooling channels for air flow. The heat transfer efficiency of aluminum exceeded other materials because of its high thermal conductivity value at 237 W/m.K that generated standardized 27.0°C air outlet temperatures enabling superior thermal uniformity alongside decreased thermal runaway risk. This high heat conductance of 401 W/m.K enabled Copper to distribute thermal energy consistently to prevent outlet temperature hot spots and achieve 27.39°C minimum outlet temperature. The low thermal conductivity value of 0.19 W/m·K in PVC led to a maximum outlet temperature of 28.0°C because it offered insufficient heat transfer while increasing thermal degradation risk. Temperature stability of the battery occurred when aluminum use maintained a continuous span from 26.6°C to 28.6°C while copper conductance yielded a range of 27.6°C to 28.2°C and PVC operation stayed within 26.8°C to 27.2°C. The laboratory analysis verifies aluminum and copper as fundamental battery constituents which provide thermal protection while accelerating heat transfer operations. The research plans upcoming experimental research as part of combined cooling endeavors to develop enhanced Battery Thermal Management Systems (BTMS) functionality in EV applications for improved operational efficiency and safety results.

1. INTRODUCTION

Lithium-ion batteries (LIBs) are crucial energy storage technology, widely employed in automotive industry to provide power for electric and hybrid vehicles. They have attracted considerable attention due to their high energy density, efficiency, voltage, lifetime, and little self-discharge rate. However, LIBs effective use requires rigorous thermal management: Operating temperatures must consistently monitored and maintained within designated range [1]. Temperature fluctuations affect chemical reactions in batteries and their individual components properties. Electrodes and electrolytes ionic conductivity illustration, which fluctuates with temperature variations [2]. Decrease in temperature leads to an increase in electrolyte viscosity, hence resulting in a reduction in ionic conductivity. The internal resistance will increase due to elevated impedance to chemical ions directed flow [2]. Moreover, several experimental investigations [2, 3] have shown that increase in charge-transfer resistance in LIBs results in performance decline at low temperatures. Multiple studies [2, 4] suggest that exposure to low temperatures may lead to decreases in power and energy densities. Furthermore, available capacity, which governs LIBs Charge State (SOC), was seen to decrease by about 20% when operating temperature reduced from 25°C to -15°C [2]. Increased temperatures also affect LIBs operation and typically cause irreversible changes. Elevated operating temperatures frequently accelerate thermal aging and may diminish LIBs longevity [1, 2, 5].

Increased temperatures are associated with the hazardous occurrence of thermal runaway, defined unregulated exothermic sequence processes. When unregulated heat production exceeds battery's thermal dissipation capacity, explosion may occur [6]. The ideal operating temperature range for LIBs is typically defined as 15-35°C, with a maximum permissible temperature of 50°C. The precise functioning range depends on cell chemistry. LIBs in electric vehicles (EVs) have garnered considerable attention as sustainable approach to reducing global carbon emissions and decreasing reliance on non-renewable energy sources [7].

Nonetheless, EVs widespread adoption faces several challenges, including high starting costs, limited driving range, inadequate infrastructure, and safety concerns [8]. LIBs are preferred energy storage solution for powering these vehicles because to their high specific energy and power density. However, LIBs performance and lifespan significantly influenced by temperature variations, necessitating effective Battery Thermal Management System (BTMS) to maintain optimal battery functionality and ensure safety [9]. This is essential from both technological and economic perspectives, Li-ion batteries undergoing thermal runaway due to insufficient BTMS, potentially obstructing recycling initiatives for sustainable future [10].

Conventional BTMS utilize heat pipes with air and liquid cooling techniques. However, these approaches limited in their ability to efficiently dissipate heat from battery pack, resulting in thermal management challenges [11]. EVs batteries essential components LIBs are frequently employed in EVs because of their high energy density, long lifespan, and lower environmental impact [12]. LIBs generate heat during both charging and discharging processes, resulting in swift rise in temperature within battery pack due to inability to dissipate heat effectively [13]. Increased temperatures significantly affect thermal efficiency and batteries lifespan, while localized high temperatures can intensify temperature variations within battery packs, consequently reducing individual cells service life. Furthermore, heat accumulation within an individual battery can trigger exothermic chemical reactions series, leading to swift rise in battery temperature [14].

Variations in ambient temperature across global regions result in LIBs operating within 20 to 60°C temperature range [15]. In contrast, air-cooling and outer case demonstrate reduced specific heat capacity and thermal conductivity relative to liquid system, resulting in an inefficient heat transfer process. Cooling fin effectively improves heat dissipation and reduces elevated temperature within battery pack. Outer case serves as passive cooling system, employing its latent heat capacity to dissipate heat produced by battery and maintain temperature regulation. Numerous studies have concentrated on improving outer cases thermal conductivity by attaching fins to battery cells surfaces [16, 17]. Battery cells commonly organized in series or parallel configurations accommodate different energy requirements, resulting in battery pack or system. LIBs function effectively within 15 to 40°C temperature range, contingent upon specific battery type, with permissible temperature variation less than 5°C. BTMS crucial for batteries packs or systems to sustain an optimal operating temperature range and mitigate thermal problems, such as cell dissimilarity and progressive aging effects [18-20]. In practical scenarios, specific improper conditions, such mechanical, electrical, and thermal abuse lead to abnormal temperature levels. An exothermic reaction transpires when battery temperature surpasses designated threshold, leading to heat accumulation [21].

2. CFD MODELLING

This study utilizes commercial CFD software ANSYS-Fluent 2022 R2 to model battery thermal behavior and to replicate temperature distribution within batteries pack. Batteries pack comprising 24 cells employed, featuring an air-cooling BTMS outlet, as illustrated in Figure 1. A and B. Behi et al. [22] performed experiments with 2 mm cell spacing and 2 m/s air velocity. 24 cylindrical cells battery pack consists arranged in parallel-series configuration, with 54 holes distributed across 6 rows and 9 columns on inlet surface. This study evaluated three materials aluminum, copper, and PVC effects on battery cells cooling efficiency and their external temperature. The battery pack dimensions are 122 mm × 82 mm × 65 mm, with each inlet hole measuring 9.5 mm in diameter. Table 1 summarizes single battery cell key parameters and its outer case.

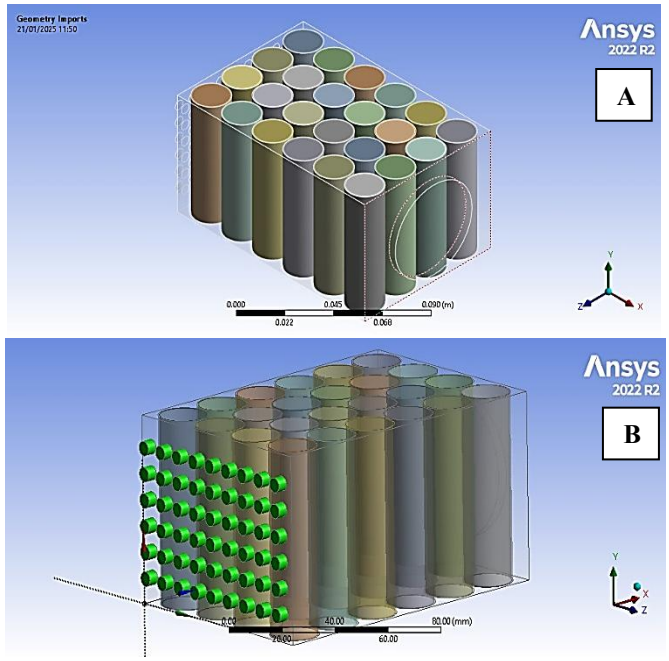

Figure 1. ANSYS model: (A) cells and outlet, (B) cells and inlet tubes

Table 1. Parameters and properties of the battery cell, outlet and outer case

Parameters of Battery Cell		
Specific heat capacity	**Density**	**Anisotropic thermal conductivities**
1200 J.kg^{-1} K^{1}	2722 kg.m^{-3}	kr = 0.2 W.m^{-1} K^{-1}, kz = 37.6 W.m^{-1} K^{-1}
(Al) outer case parameters		
Specific heat capacity	**Density**	**Thermal conductivities**
900 J.kg^{-1} K^{1}	2710 kg.m^{-3}	237 W. m^{-1} K^{-1}
(Cu) outer case parameters		
Specific heat capacity	**Density**	**Thermal conductivities**
392 J.kg^{-1} K^{1}	8900 kg.m^{-3}	401 W. m^{-1} K^{-1}
(PVC) outer case parameters		
Specific heat capacity	**Density**	**Thermal conductivities**
600 J.kg^{-1} K^{-1}	100 kg.m^{-3}	0.1 W.m^{-1} K^{-1}

CFD modelling basically predicated on fluid dynamics governing equation. These equations embody of physics conservation rules mathematical formulation. The CFD model represents fluid flow processes fundamental characterization [23, 24]. The suitable numerical physical boundary condition representation is contingent upon governing equations mathematical formulation and numerical technique employed [25, 26]. The governing equations encompass mass conservation, momentum, and energy, articulated as follows: Mass conservation equation:

$$\rho a\left(\frac{\partial}{\partial t}+\nabla\vec{\vartheta}\right)=0 \tag{1}$$

Momentum conservation equation:

$$\frac{\partial\left(\rho_a\vec{\vartheta}\right)}{\partial t}+\nabla\left(\rho_a\vec{\vartheta}\,\vec{\vartheta}\right)=-\nabla\,\rho_a \tag{2}$$

Energy conservation equation:

$$\frac{\partial\left(\rho_a C_{pa} T_a\right)}{\partial t}+\nabla\left(C_{pa}\,\rho_a\vec{\vartheta}\,T_a\right)=\nabla\left(K_a\nabla\,T_a\right) \tag{3}$$

These governing equations employed in finite elements computing operations or finite volume methodologies. In these equations, letters *r*, C_p, *T*, *P*, and K represent density, specific heat, temperature, pressure, and heat conductivity coefficient, respectively. Letter *a* in subscript form indicates cooling air. Governing equations can also be used for battery cell. To be more precise, the energy equation may be expressed in following way:

$$P_p\,C_{pb}\frac{\partial T}{\partial t}=\nabla\left(K_b\nabla\,T\right)+q \tag{4}$$

where, *q* is heating production rate for each single battery unit volume and subscript *b* refers to battery cell. Additionally, CFD approach offers turbulent flow numerical solution. Shear-stress transport *k*-ω model replicates turbulent flow that occurs during battery pack cooling phase. *k*-ω model has made turbulence model more accurate when it comes to forecasting free shear flows. Two main components, turbulent kinetic energy *k* and specific dissipation rate w, computed using transport equations below [27]:

$$\frac{\partial}{\partial t}(\rho k)+\frac{\partial}{\partial x_i}(\rho k u_i)=\frac{\partial}{\partial x_j}\left(\Gamma_k\frac{\partial k}{\partial x_j}\right)+G_k-Y_k+S_k+G_b \tag{5}$$

$$\frac{\partial}{\partial t}(\rho\omega)+\frac{\partial}{\partial x_i}(\rho\omega u_i)=\frac{\partial}{\partial x_j}\left(\Gamma_\omega\frac{\partial\omega}{\partial x_j}\right)+G_\omega-Y_\omega+S_\omega+D_\omega+G_{\omega b} \tag{6}$$

G_k stands for the turbulent kinetic energy creation, whereas G_w stands for particular dissipation rate development *w*. *G*, *Y*, and *S* stand for effective diffusivity, dissipation, and user-defined source terms, respectively. The term "d_w" is an abbreviation for "cross-diffusion." In addition, G_b and G_{wb} take into consideration buoyancy terms. The CFD program calculates all of the terms throughout the simulation procedure.

3. MESH INDEPENDENCE ANALYSIS

Prior research unequivocally demonstrates that mesh quality is a pivotal factor influencing the realism and reproducibility of simulations performed in ANSYS. The generation of a mesh divides the geometry into discrete elements, enabling the solver to estimate solutions to diverse physical issues. Accurate meshes provide a more precise representation of the model's actual behavior, minimizing discretization errors and improving convergence in the solution phase [28]. Inferior meshes, marked by irregular shapes, high aspect ratios, or distorted features, might result in erroneous solutions, numerical oscillations, and even solver malfunction. The mesh sensitivity analysis is crucial for achieving accurate and reproducible numerical results; thus, authors must guarantee that the findings are unaffected by mesh refinement. This process entails generating a new set of meshes with an increased number of components or superior quality and performing a simulation on each one. The results, including temperature and other pertinent output properties, are then compared using the designated meshes [29]. If the results stabilize and become more precise, they are considered mesh-independent. This confirms that the mesh in this simulation is adequately developed to provide a comprehensive and precise representation of the physical processes while reducing computing resource usage. The mesh procedure for this study begins with configuring the selected mesh size and method for the entire body to improve mesh accuracy according to the parameters outlined in Figure 2 for all model surfaces. The mesh elected started with 3.5 mmm element size as begging, then reduced it by 0.5 mm in every step. The results in Figure 2 illustrated a stable outlet temperature when the mesh element size between (0.5 to 1.5 mm), after these sizes a big divergent can noticed in outlet results, the authors chose 1.5 mm element size for this study with 1042486 elements number and 605876 nodes in the three simulation models. The mesh for the three models illustrated in Figure 3 below.

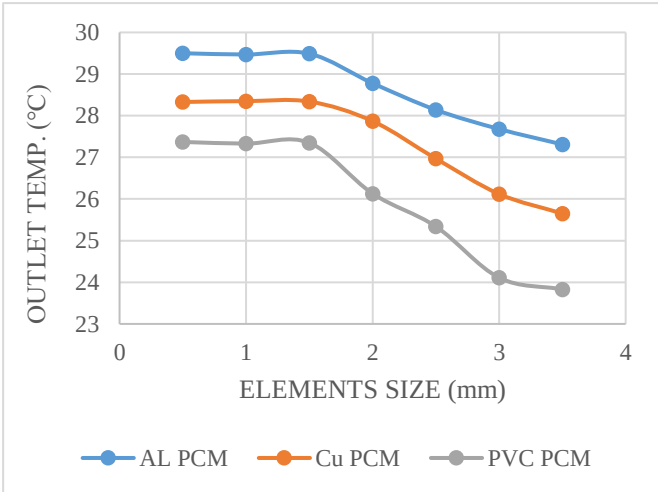

Figure 2. Mesh independence analysis

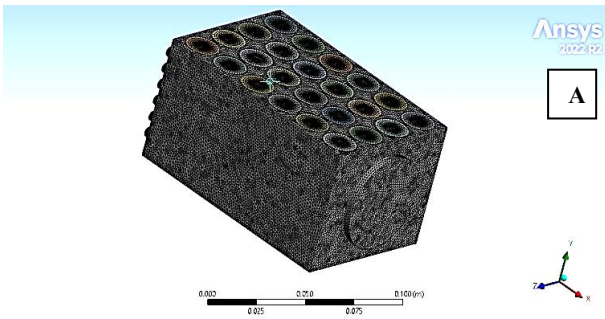

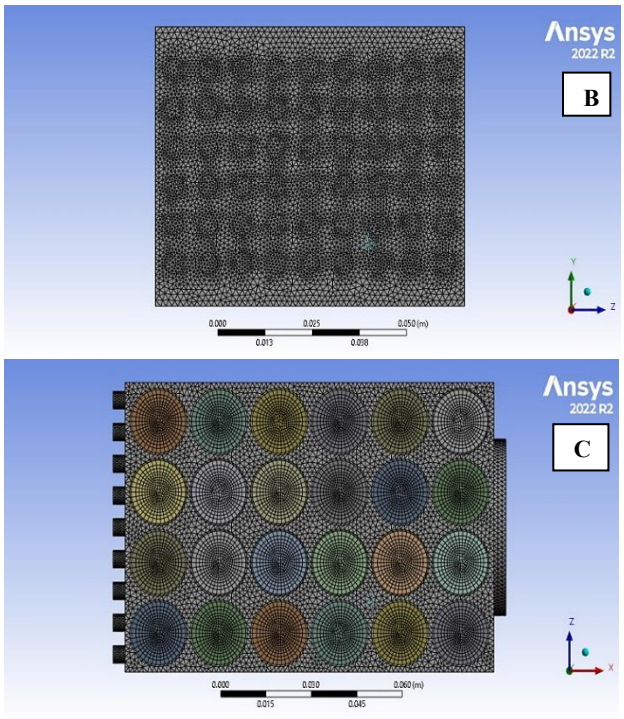

Figure 3. Simulation model ANSYS mesh: (A) geometry mesh, (B) inlet mesh, (C) battery and outer case mesh

4. NUMERICAL METHOD

Cases were modeled and solved using ANSYS FLUENT software version 2022 R2. segregated, implicit solver option is utilized to solve governing equations. The first step is to create algebraic equations system by discretizing mass governing equations, momentum, and scalar transport. The finite volume method is specific numerical approach for finite differencing and is the most often used method for flow computations in computational fluid dynamics (CFD) algorithms [30]. This section explains the fundamental steps that are part of finite volume computations. In this study, the k-epsilon turbulence model was used to account for flow variations caused by turbulence. The RANS equations were discretized instead when instances were run. When equations were discretized using the appropriate differencing scheme for expressing differential expressions in upwind or other higher-order differencing schemes, the integral equation was used, which included the discrimination scheme terms in energy, momentum, and turbulence parameters. The resulting algebraic equations were solved at each cell node [31]. The value of interest scalar characteristics, such as temperature at a certain place in the computational domain, is determined by the direction and velocity of the flow, which must also be solved during the calculation process. The segregated solver, which is a sequential approach for solutions, takes less memory than the linked solver when employed in numerical computing. The SIMPLE method is employed in the computation procedure for this project. The standard pressure interpolation system and SIMPLE pressure velocity connection have been put into action. For CFD simulations with 500 iterations, the residual root-mean-square (RMS) goal value was $10^{-2.5}$ for continuity and 10^{-6} for the energy equation, as shown in Figure 4 below.

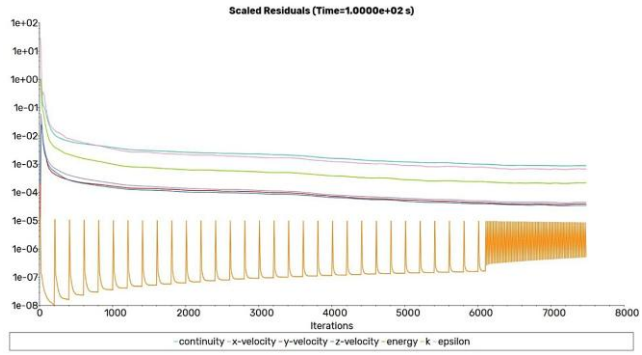

Figure 4. Fluent simulation scaled residuals solution

5. RESULTS AND DISCUSSIONS

5.1 Heat distribution models

During thermal runaway propagation, extra heat generated due to complex charging exothermic reactions, and thermal runaway cell temperature increased dramatically. Lopez et al. [32] captured this feather experimentally. Based on experimental data, authors applied temperature of thermal runaway cell, but this study used natural air ventilation without fan to simulate outer case material effects on heat distributions and outlet air temperature. By using this thermal approach, current case successfully simulates scenario with cell experiencing thermal runaway. The case layout is same as pre-mentioned case, shown in Figure 5(A), (B), and (C).

The heat propagation inside the battery pack was clearly presented in Figure 5. the heat generation per unit volume for the batteries were 48750 W/ m^3. Compared Al outer case outlet air temperature in Figure 5(A) to copper and PVC outer case in (B) and (C), illustrated increasing in battery cell temperature distribution with Cu outer case. Also illustrated changed in temperature distribution of the outer air-cooling case the outlet temperatures of the three models were 27.0℃ for the Al outer case, 27.39℃ for the Cu outer case, and 28.0℃ for PVC outer case. Figures 6 and 7(A), (B), and (C) shows the outlet heat distribution of the three models with its average temperature.

Aluminum outer case in Figure 6(A) shown the lowest outlet temperature due to the high battery cells heat distraction toward the aluminum outer case walls and high aluminum conductivity which produced low outlet temperature. Aluminum performs heat transfer efficiently at rates of 237 W/m·K which produces swift heat removal from the system. The uniformity of temperature distribution improves because aluminum enables fast heat removal from the battery pack. The material stops the formation of aggressive heat points that cuts down thermal stress and enhances battery cell durability. Along with its stronger thermal conductance value of 401 W/m·K copper surpasses aluminum's performance potential in thermal distribution. The increased outlet temperature points to specific heat capacity together with outer case distribution effects beyond just thermal conductivity. Practical battery applications are potentially limited by both the heavier weight and denser composition of copper. Relative to PVC demonstrates exceptionally low thermal conductivity that reaches values of about 0.19 W/m·K. The material's low conductivity creates obstacles to heat transfer, which results in elevated outlet temperatures and poor cooling performance. The gradient slope of temperature reveals uneven heat dissipation patterns along with possible local hotspots in the

system that pose overheating risks. While PVC does not function as regular outer case, it could be incorporated within composite structures that potentially increased outlet temperatures.

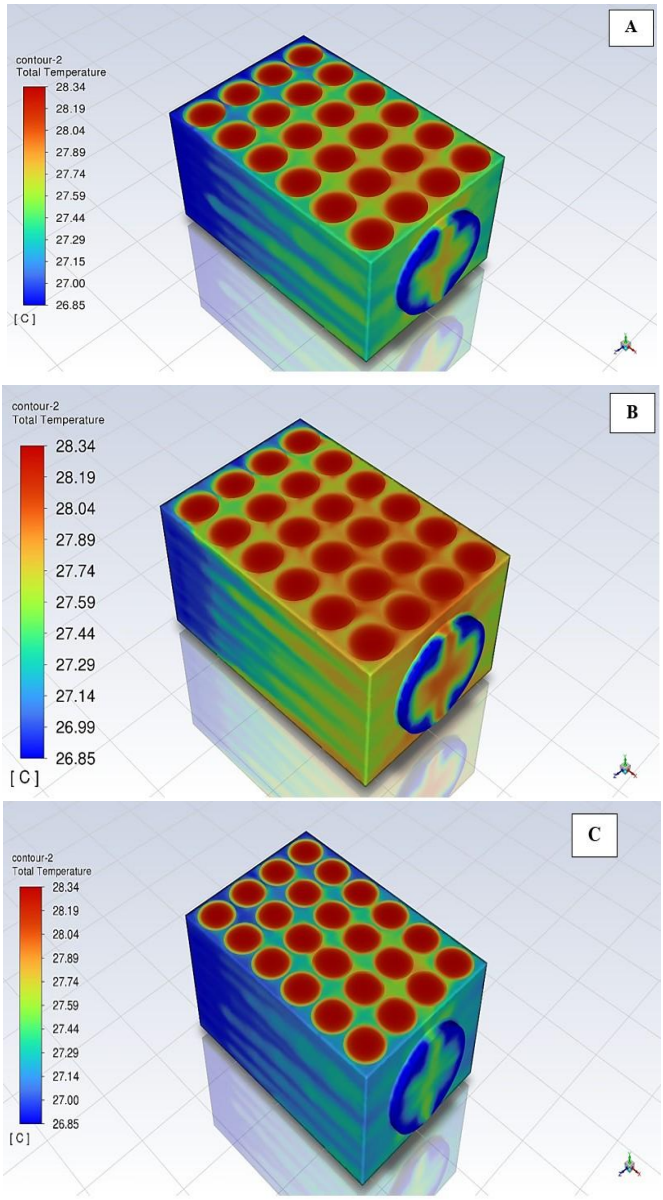

Figure 5. Outer case and battery pack heat distribution: (A) Aluminum outer case, (B) copper outer case, (C) PVC outer case

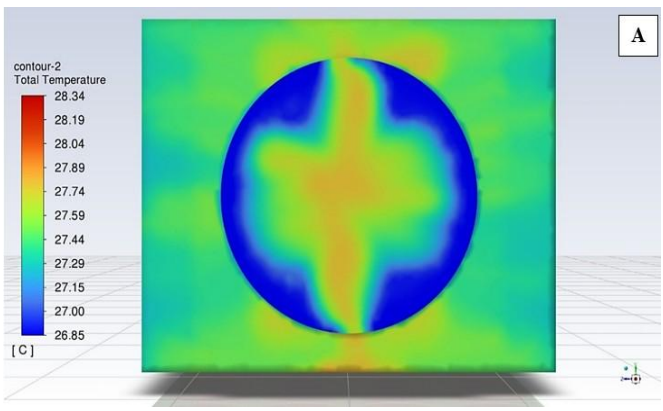

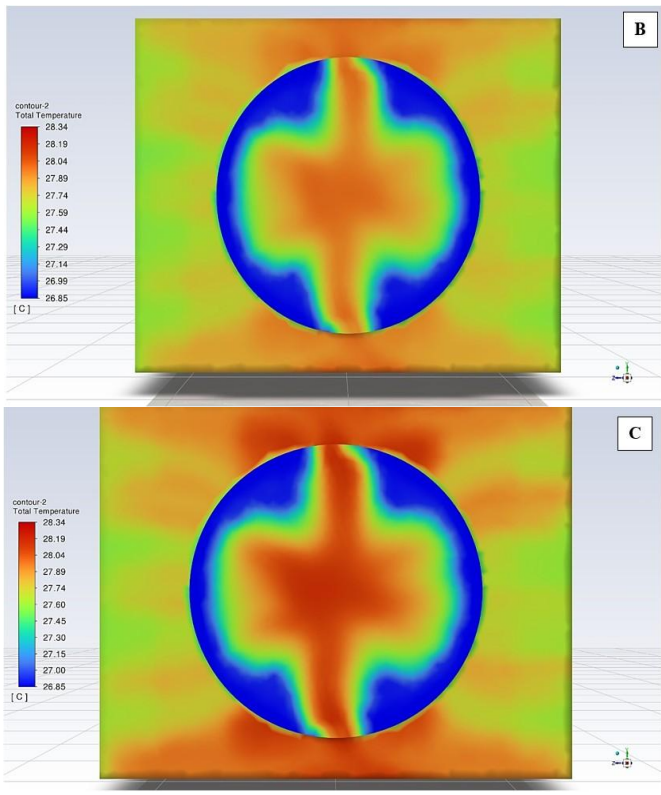

Figure 6. Outer case and battery pack outlet heat distribution: (A) Aluminum outer case, (B) copper outer case, (C) PVC outer case

Heat dissipation efficiency depends on the thermal conductivity properties of selected outer case that adjusts outlet temperature levels. The outlet temperature data in above Figure 7 reveals PVC produces the highest readings while copper gives intermediate results but aluminum demonstrates the lowest temperatures throughout the outlet length. Thermal energy peaks at its highest point in PVC (Polyvinyl Chloride) material indicating its heat dissipation performance resides among the lowest. Heat remains trapped inside the system so outlet temperatures rise. Copper (Cu) outlet temperature performance balanced values because its high thermal conductance allows effective heat dissipation. The thermal management capabilities from PVC arrive lower than those of PVC. The thermal conductivity properties of aluminum produce the most uniform outlet temperature distribution. Aluminum superiorly positions itself above copper and PVC because enhanced heat transfer operations produce lower outlet temperatures. Every material shows temperature increases for the first instance before reaching maximum points just beneath the center of the outlet (0.03-0.04 m) before the temperature descends. This behavior likely corresponds to the heat accumulation and subsequent dissipation dynamics within the outer case. Initial region (0.01-0.03 m) temperature increase occurs due to battery heat because the material absorbs heat energy. Mid region (0.03-0.04 m) this peak location signifies when thermal storage reaches equilibrium with heat transfer thus reflecting outer case thermal saturation at that point in the zone. Final region (0.05-0.07 m), the material's efficient thermal energy transfer pattern creates temperature reduction which allows heat to move towards the outlet. Outer case's thermal conductive ability correlates with their ability to preserve lower outlet temperature levels directly. Thermal regulation processes within PVC remain highly inefficient which results in wide temperature range

changes at the outlet. The thermal regulation provided by Aluminum results in a narrower temperature span when measured from the inlet to the outlet.

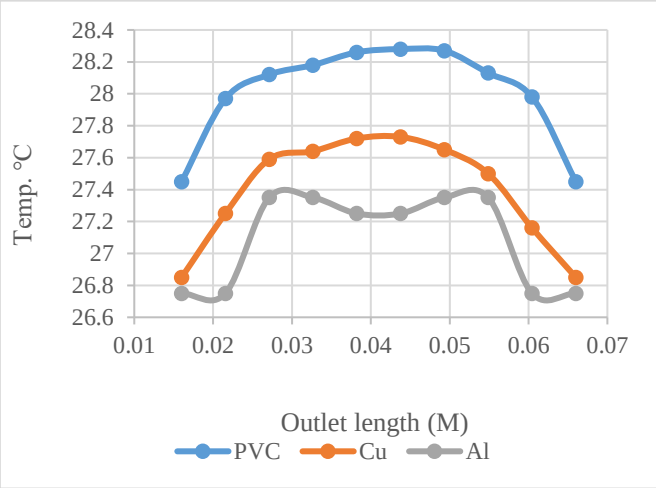

Figure 7. Outer case and battery pack outlet heat distribution diagrams: (A) Aluminum outer case, (B) copper outer case, (C) PVC outer case

5.2 Outer cases heat distribution models

Thermal properties of aluminum and copper produce high-quality cooling effects through efficient conduction. The reduced thermal conduction of PVC produces batteries with uneven temperature distribution across specific regions of the package. A comprehensive evaluation of temperature patterns remains absent for complex battery configurations that use multiple materials. Temperature generated within operating battery cells threatens to cause thermal runaway and decreases performance alongside accelerated service life degradation. The outer casing material represents a vital thermal behavior element of a battery system because it provides insulation while functioning as a heat release channel [33]. Thermal conductivity together with heat transfer abilities of the battery pack outer casing determine how temperature spreads across the cell battery groups. Different types of materials exist for battery enclosures because these enclosures show different thermal responsiveness and structural stability levels. The materials Aluminum (Al) and Copper (Cu) along with Polyvinyl Chloride (PVC) are preferred for enclosure fabrication because they show contrasting thermal conductive behavior while exhibiting varying heat dispersion capabilities and load-bearing properties. Figure 8(A), (B), and (C) illustrated the heat distributions of the outer case wall.

Figure 8 presented 24-cell battery module ANSYS-based thermal simulations enclosed within three different casing materials, aluminum, copper, and PVC. Simulation goal is to study how different casing materials affect both the heat dissipation and thermal patterns. The analysis reveals the thermal management traits of these materials so that battery packs operating within EVs and ESS systems can maximize safety alongside efficiency and product life.

The contour plots demonstrate steady-state total temperature patterns across exterior surfaces of various casing materials. The thermal performance of these cases is primarily governed by their respective thermal conductivities. Aluminum case in Figure 8(A) shows 28.273°C slightly higher average temperature. Aluminum thermal conductivity rating at ~237 W/m. K less than copper but it remains suitable for productive heat spreading functions. While aluminum distributes heat less effectively than copper it presents an acceptable solution because of its lightweight qualities and mechanical stability. Copper in Figure 8(B) case design shows the most effective heat dissipation capability with an average outer wall temperature measurement at 27.849°C. Due to its peak thermal conductivity value of around 400 W/m·K copper provides the most efficient heat transfer process from battery cells to case outer surface. The improved heat transfer reduces localized overheating inside the battery module that improves thermal uniformity and potentially extends the lifespan while enhancing safety. PVC in Figure 8(C) case shows an outer wall temperature maximum. Inspectors could find the outcome confusing at first glance. PVC thermal conductivity shows very low levels at 0.19 W/m·K although it behaves as an insulator. Heat dissipation through PVC occurs more slowly than in metals because its heat transfer operations work differently. The material exhibits poor heating conductivity that traps heat within battery compartments leading to insufficient external heat dissipation. The thermal gradients between inner battery cells and outer surface produce temperature stresses that increases safety risks and accelerates degradation in packaging [34].

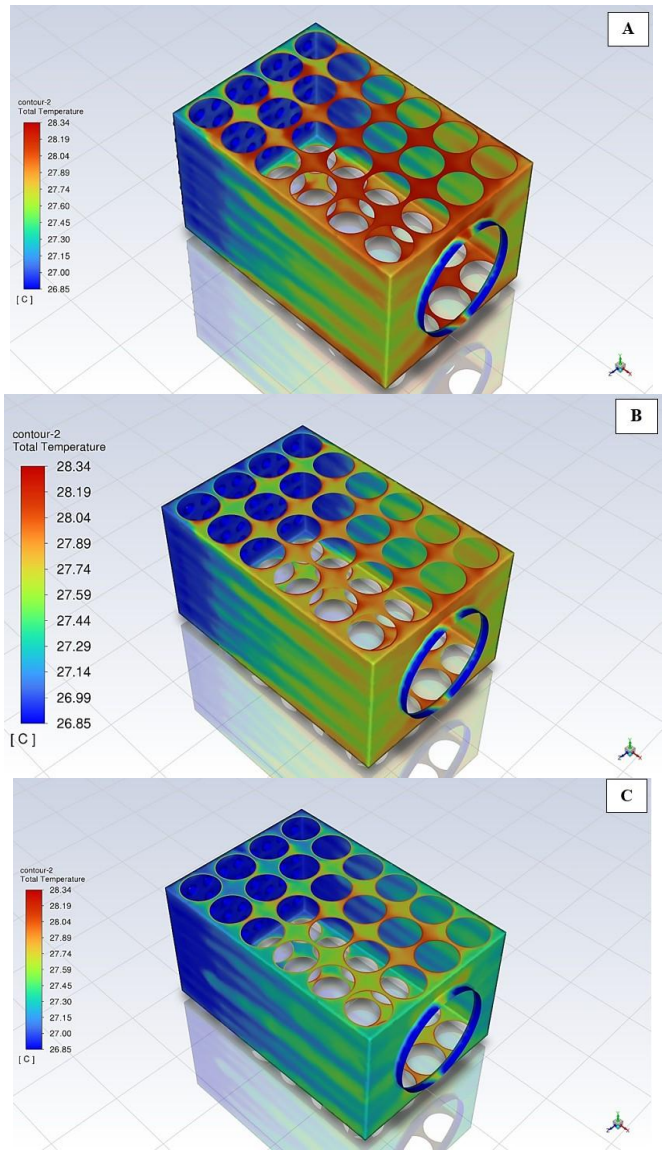

Figure 8. Outer case heat distribution diagrams: (A) Aluminum outer case, (B) copper outer case, (C) PVC outer case

Results in Figure 8 illustrated the efficient heat dissipation from Copper and Aluminum cases prevents thermal runaway failures which represent a major safety challenge for batteries. Thermal hotspots become more likely because PVC exhibits insulating properties that prevent even temperature distribution inside a battery cell. Distributed low temperature field can boost battery performance by reducing electrolyte degradation and electrical resistance formation. The most heat-conducting material enables the best thermal control system through copper but aluminum presents balanced benefits between thermal operation and weight reduction and expenditure.

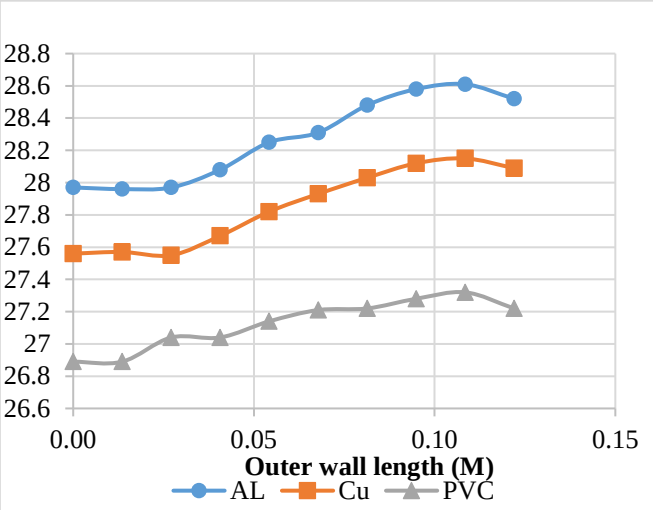

Figure 9. 24 cell battery module temperature variation along the outer wall length

Figure 9 presents the temperature variation along 24-cell battery module outer wall length. The graph shows the outer wall length in meters on the x-axis with temperature readings in ℃ spread out along the casing on the y-axis. Each material creates a unique temperature pattern since their combination of thermal conductivity and heat dissipation properties determines their behavioral output. The blue line showing aluminum registers the strongest temperature increases because its temperature gradually grows from 28.0℃ to 28.6℃ across the wall perimeter. Copper (orange line) conducted heat with superior efficiency during this experiment through its temperature range from ~27.6℃ to ~28.2℃. Data shows that PVC material (gray line) creates the coolest temperatures between ~26.8℃ and ~27.2℃ proving poor thermal conductivity of this material. Copper Exhibits the most uniform temperature distribution, with a moderate slope. Local hot spots dissipate heat quickly since copper bears the most rapid thermal conductivity to minimize temperature gradients between regions. Heat accumulation progresses in view as advanced thermal conductivity properties of materials work to decrease heat retention. The temperature range from aluminum extends more than copper that affects heat dissipation efficiency. Aluminum line demonstrates a sharper temperature slope than copper indicates heat distribution occurs less evenly throughout the casing surface. When compared to copper aluminum acts as a thermal conductor but performs at a lower level that leads to concentrated higher temperatures. PVC shown the lowest temperature range but with gradual increase along case wall length. The PVC heat constraining properties successfully control transfer between battery cells and outside materials. Under freezing external temperatures, battery modules heat performance retains stability but not heat performance directly.

The general increase in temperature along the outer wall length, particularly in the aluminum and copper cases, can be attributed to heat flux distribution and convection effects. Heat generated by battery cells travels outside through casing enclosure material. The battery emerges from the heat source with better heat dissipation at these points due to stronger temperature gradients between its surface and the external environment. Heat moves from the source to the casing wall progressively reduces heat dissipation efficiency that results in stepwise temperature increases. The dominant conduction mechanisms in aluminum and copper metals lead to a moderate heat expansion but conduction remains the primary transfer mechanism. PVC demonstrates slower heat buildup across the outside shell yet the battery cells stay hotter at interior locations. These results are very critical in system outer case materials selection. Superior thermal management applications require copper cases yet these solutions present practical challenges because they are expensive and dense and easily oxidize. Aluminum cases find widespread usage in EV battery packs because they offer a perfect combination of thermal efficiency alongside structural strength. PVC cases thermal conduction limitations make them workable for small energy systems yet difficult to utilize effectively in high-power battery applications [35].

5.3 Battery cells with different casing materials thermal performance analysis

Performance alongside long-term reliability and operational safety depends directly on effective battery thermal management solutions that are especially vital for high-power applications in EVs and energy storage systems. The selection of battery cell casings determines heat dissipation rate through their impacts on thermal conduction properties. Figure 10(A), (B), and (C) represented the thermal distribution of the battery cells for the three cases.

Figure 10(A) shows the battery cells heat distribution with aluminum outer case, aluminum finds widespread use in battery casings because it offers both excellent thermal conductivities along with being light-weight. Simulation results demonstrate that the battery cells maintain a generally moderate temperature profile where maximum heat sits at the cell tops while temperatures decrease from top to bottom. The heat dispersal ability of aluminum casing becomes evident through its even distribution of red and yellow areas throughout the battery cell area. Heat dissipation occurs towards the surrounding environment according to blue regions observed in the bottom sections. Figure 10(B) indicate the battery cells inside copper outer case provides the best temperature distribution while maintaining a reduced gradient between cell temperatures. A closer look at the upper red zones in the top section shows minimal differences compared to the aluminum. model whereas the blue regions assume fewer numbers thus indicating superior lateral heat distribution properties. The improved conductive properties of copper lead to even temperature distribution throughout all battery cells. Figure 10(C) results demonstrate batteries inside PVC case generate significantly steep temperature gradients across their length shown by distinct blue lower sections followed by red intense regions at the top. The results show poor heat dissipation causing extreme temperature increases at cell battery. Because PVC has poor thermal conductivity

properties, it accumulates heat which renders it unfit for high-power applications requiring effective thermal dissipation.

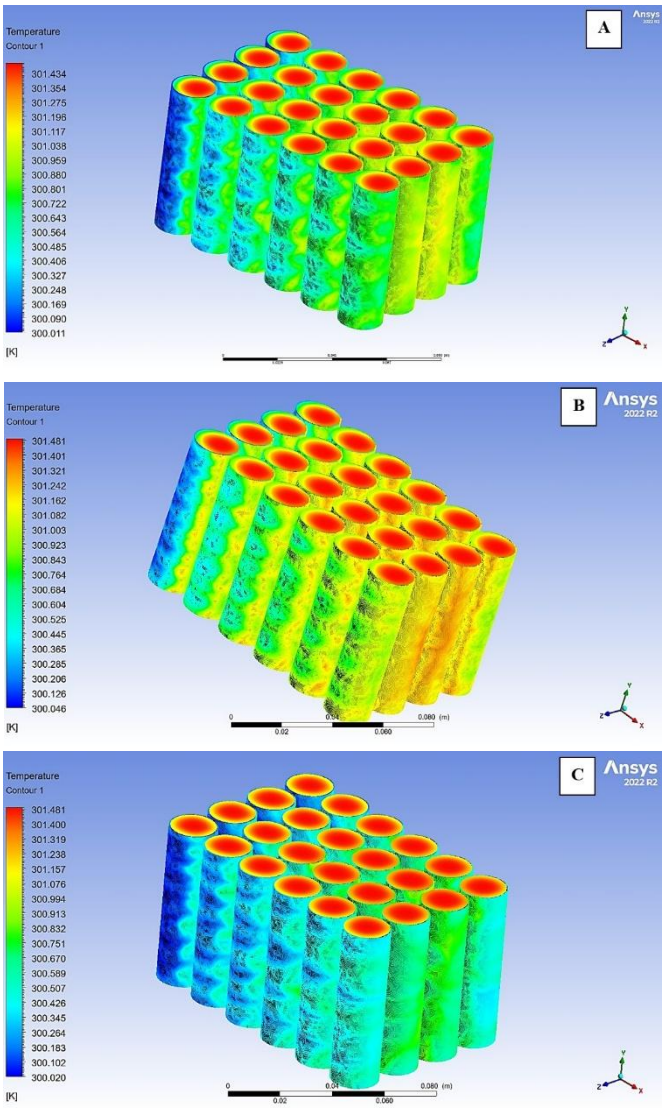

Figure 10. Batteries cells heat distribution models: (A) Al outer case, (B) Cu outer case, and (C) PVC outer case

5.4 Heat transfer mechanisms

The evaluation of heat transfer within the battery pack occurred by investigating conduction together with convection and radiation processes. Throughout the entire heat transfer process conduction served as the primary method for heat transport from battery cells to outer casing for every material. Temperature losses through the materials differed because of their distinct conductive properties. The energy conservation equation is given in (3), Since heat is primarily dissipated through conduction and convection, the overall heat transfer coefficient (U) is defined as:

$$\frac{1}{U} = \frac{1}{h_{air}} + \frac{L}{h_{case}} + \frac{1}{h_{air,out}} \tag{7}$$

where: h_{air} is the convective heat transfer coefficient of cooling air (~50 W/m²K for turbulent flow), k_{case} is the thermal conductivity of casing materials (Al: 237 W/m·K, Cu: 401 W/m·K, PVC: 0.19 W/m·K), L is the casing thickness. The material used for the outer casing primarily determines how fast heat escapes from the system. Each material's heat dissipation capability is evaluated through the Biot number (Bi) definition as:

$$B_i = \frac{hl_c}{K} \tag{8}$$

where: h is the convective heat transfer coefficient, L_c is the characteristic length, K is the thermal conductivity of the outer casing. According to Eq. (8), Bi for aluminum will be 0.00063, 0.00037 for copper, and 0.79 for PVC. The Biot number for aluminum and copper remains much lower than (1) which allows interior heat conduction to happen significantly faster than surface heat transfer allowing for uniform temperatures inside the casing. PVC demonstrates a high Biot number value because of its strong internal thermal resistance which produces uneven temperature gradients throughout the material resulting in thermal hotspots. The effectiveness of different casings is analyzed using thermal resistance (Rt):

$$Rt = \frac{1}{hA} + \frac{L}{kA} \tag{9}$$

The effective heat dissipation surface area is represented by A. The evaluation of cooling effectiveness occurs for a battery pack with dimensions 122 mm × 82 mm × 65 mm as shown in Table 2. Results indicate aluminum stands as the most practical option for EV applications because it combines the suitable thermal properties with lightweight construction and inexpensive materials. Although superior in conductivity, copper possesses density together with higher cost that makes its use impractical for battery container applications. The thermal inefficiency of PVC creates outlet temperatures that go higher which elevates the risk of thermal runaway.

Table 2. Cooling effectiveness and thermal resistance analysis

Material	Thermal Conductivity (W/m·K)	Thermal Resistance (Rt)	Temp. Rise
Aluminium	237	Low	27.0
Copper	401	Very Low	27.39
PVC	0.19	High	28.0

5.5 Flow field analysis

This study uses convection to cool the battery pack through inlet tubes that allow air to pass over the battery cells. Lower velocity distributions in cooling air reduce the performance of thermal dissipation from battery cells. The airflow inside the battery pack obeys the Navier-Stokes equations which preserve both mass conservation and momentum conservation rules:

$$\frac{\partial \rho}{\partial t} + \nabla.(\rho v) = 0 \tag{10}$$

where, ρ is the air density and v is the velocity vector. Momentum conservation or (Navier-Stokes equation) will be as follow:

$$\frac{\partial(\rho v)}{\partial t} + \nabla.(\rho vv) = -\nabla P + \mu\nabla^2 v \tag{11}$$

where, P is the pressure and μ is the dynamic viscosity of air.

The Reynolds number (Re) determines the nature of the airflow inside the cooling channels:

$$Re = \frac{\rho v D}{\mu} \quad (12)$$

The hydraulic diameter D of the airflow channel exhibits a measurement relationship with the characteristic velocity v. The airflow transitions to turbulent flow at Reynolds numbers greater than 4000. A turbulent flow transition becomes more probable when using 9.5 mm channel width together with 2 m/s inlet velocity. The turbulent system requires modeling through the k-ω Shear-Stress Transport (SST) model for simulation purposes.

6. VALIDATION

Temperature proper management plays an essential role in protecting both the functioning and safety and lifetime expectancy of LIBs throughout EVs. The current analysis evaluates research findings about BTMS by cross-comparing data from recent experiments against past peer-reviewed scholarship to validate this research results. The current study utilizes a CFD simulation to examine air-cooled BTMS thermal characteristics with different outer case materials. Experimental validation and error rates for simulation results remain absent alongside temperature uniformity (ΔT) specifications within the battery pack. The BTMS-DRC thermal management system which uses a dual-evaporator vapor compression refrigeration system with refrigerant cooling medium is investigated in the research report titled " Investigation of the Performance of Battery Thermal Management Based on Direct Refrigerant Cooling: Simulation, Validation of Results, and Parametric Studies" [36]. Under 160-320 W heat generation system operates to keep battery module temperatures at or below 35℃ with a uniform temperature distribution (ΔT) between 1.7 to 4.2℃. In (BTMS-DRC) system using a refrigerant as the cooling medium. The device operated at of ≈28.6℃ outer case temperature with the aluminum outer case material. The specific design enabled consistent heat dispersion that avoided temperature concentrations on specific points. The battery heat moved efficiently from the internal cells to the air-cooling system through conductivity that minimized thermal strain on the cells. The outer case temperature of Copper Case experienced an even spread of heat from 27.6℃ to 28.2℃. The combination of higher conductivity and denser structure and specific heat capacity slowed down heat dissipation in copper. Temperature measurements at the outlet showed that the Copper case kept more heat compared to Aluminum because it reached 27.39℃ while Aluminum reached 27.0℃. Temperature measurements showed that the PVC Case functioned well as an insulator by raising the battery case temperatures between 26.8℃ to 27.2℃. Excessive heat developed in the battery due to inadequate heat conduction leading to performance problems. Insufficient cooling operations caused the outlet temperature to reach 28.0℃. Table 3 summarize these research parameters.

The outlet temperature maintained stability below 35 degrees Celsius regardless of which outer case material was chosen during Refrigerant Cooling BTMS measurements in the study of Jamsawang et al. [36]. The temperature uniformity measured as ΔT consistently stayed within 4.2 degrees Celsius that exceeded air cooling performance levels. Refrigerant-based cooling effectively reduces the significance of outer case materials as main contributors to heat elimination systems. Table 4 summarize Jamsawang et al. [36] research parameters.

Table 3. Outlet temperature from air-cooled BTMS (current study)

Outer Case Material	Thermal Conductivity (W/m·K)	Outlet Air Temperature	Battery Pack Temperature
Aluminium	237	27.0℃	26.6-28.6℃
Copper	401	27.39℃	27.6-28.2℃
PVC	0.19	28.0℃	26.8-27.2℃

Table 4. Outlet temperature from refrigerant-cooled BTMS

Condition	Max Module Temperature (℃)	ΔT (Uniformity)
Heat Load: 80W	≤35	1.7℃
Heat Load: 320W	≤35	4.2℃

A comparison between the results of the two research to validated the results of this work. The results illustrated in Table 5 below.

Table 5. Cooling system efficiency (air cooling vs. direct refrigerant cooling)

Feature	Air-Cooled BTMS	Refrigerant-Cooled BTMS
Cooling Mechanism	Forced air circulation	Phase-change refrigerant cooling
Outer Case Influence	High impact on temperature	Minimal impact
Temperature Uniformity (ΔT)	2.0-3.4℃	1.7-4.2℃
Outlet Temperature Stability	Varies with material (27.0-28.0℃)	Maintained ≤35℃
Thermal Runaway Risk	Higher in PVC cases	Lower due to refrigerant heat absorption

Figure 11 (A) and (B) illustrated the outer case temperature distribution of the two systems, these images evaluate BTMS temperature distributions resulting from two cooling techniques applied to various outer case materials (Al, Cu, and PVC). A first image shows temperature contours depicting Aluminum (Al), Copper (Cu) and Polyvinyl Chloride (PVC) outer cases when composites with air-cooled BTMS. The research examines the effects of various material thermal conductivities on battery pack temperatures at their highest and lowest points together with heat dispersal uniformity levels. Secondly, the temperature distribution image displays Silver, Copper, Aluminum, and Brass outer cases under direct refrigerant-cooled BTMS regulation. Better thermal regulation across the battery module can be achieved through the combination of latent heat absorption alongside convective cooling mechanisms.

The results of the figure shown that the maximum temperature inside Aluminium outer case reaches 3.55% higher under refrigerant cooling than air-cooling conditions do. Under refrigerant cooling conditions, the minimum

temperature drops by 3.54% while the maximum temperature of copper rises by 2.52%. The cold temperature readings indicate a slight enhancement in stability because they registered 1.66% reduction compared to previous results. The maximum brass temperature under refrigerant cooling exceeds the PVC maximum temperature by 11.40%. The refrigerator cooling method produces minimum temperatures that are 8.15% colder than typical temperatures. This result validated this research results.

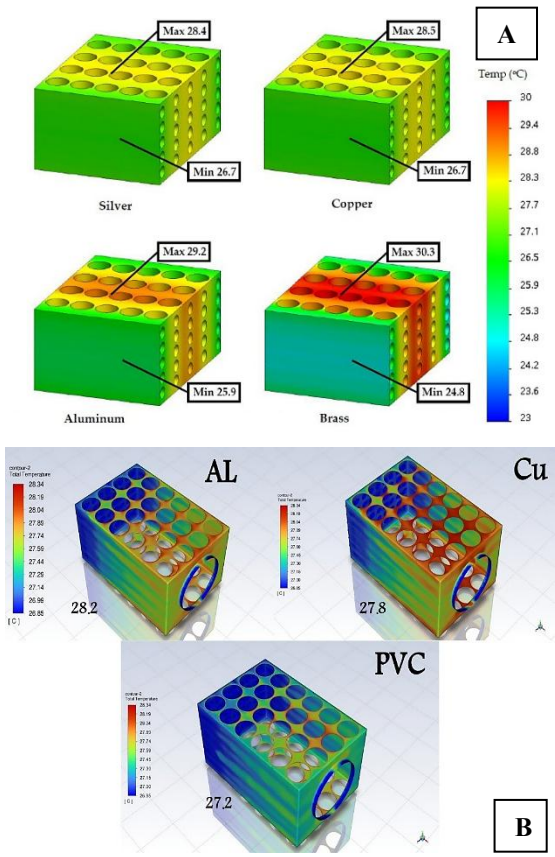

Figure 11. The outer case heat distribution: (A) Jamsawang et al. [36], (B) The current study

7. POTENTIAL LIMITATIONS AND BIASES

The research examines a simulated 24 cells battery pack consisting. The research delivers helpful results yet obstacles emerge when obtained data to electric vehicle (EV) and energy storage system (ESS) battery systems. The simulation parameters cannot accurately represent the complex behavior of large-scale systems because multiple cells in large packs follow different heat dissipation patterns. Further investigation is needed to study the thermal behaviors of bigger cell arrangements because their interactions remain poorly understood. Real-world accuracy in scaling the results might be compromised due to this issue.

The paper examines the selection of Aluminum (Al), Copper (Cu), and PVC for outer case materials but lacks information about environmental consequences during production, usage, and disposal of these materials. The excellent thermal capabilities of copper come at a resource and environmental cost because the material requires extensive amounts of resources and creates greater carbon emissions than aluminum. The lighter weight and economical nature of PVC presents environmental problems because of its restricted recyclability potential and hazardous properties toward the environment. The article lacks a comprehensive assessment of material environmental impacts through life cycle assessment evaluation although this investigation does not examine the issue thoroughly.

The research depended on ANSYS Fluent 2022 R2 simulations to generate findings that used specific controlled parameters for battery pack arrangement together with environmental settings and cooling elements. The implementation in actual use environments results in substantial condition variations. Various environmental temperatures alongside aging battery cells along with vehicular movement and air circulation affect how the battery heats up. The method of air-cooling in the study lacks effectiveness for large electric vehicle battery systems operating under different climatic conditions or high-power demands. Testing through real operational settings and hybrid cooling systems needs to be performed to examine how results perform safely under changing environmental conditions.

8. CONCLUSIONS

Research into lithium-ion battery (LIB) thermal management reveals how essential BTMS are for superior performance along with extended lifetime and safety protection. The fluctuating temperatures that affect battery efficiency and power density as well as change the lifespan require improved thermal management techniques for sustainable energy storage and electric vehicle applications. The key findings from this CFD modeling are:

(1) Aluminum outer case used as heat disseminator achieved 237 W/m·K thermal conductivity resulting in outlet air temperature 27.0℃ with even heat distribution in the battery pack. The aluminum casing successfully conducted heat away from the battery pack while preserving the system's lightweight design so it worked well for thermal management needs.

(2) 401 W/m·K copper thermal conductivity produced 27.39℃ exit air temperature leading to most even temperature distribution when compared to other cases. This fast heat transfer ability lowered potential localized overheating risks but the substance's denser matter combined with higher price presents obstacles for use.

(3) PVC used as conductor material demonstrated the highest outlet air temperature at 28.0℃ due to its 0.19 W/m·K thermal conductivity value. The heat dissipation ability proved inadequate. The study showed steep temperature differences and an elevated risk for localized overheating.

(4) The battery pack temperature utilizing aluminum fell between 26.6℃ and 28.6℃ while copper maintained a consistent temperature range of 27.6℃ to 28.2℃. The PVC materials displayed significant variations in temperature between 26.8℃ and 27.2℃ that reflected their suboptimal thermal conductivity rates.

(5) Battery cell in aluminum responded with a less dramatic thermal profile yet the cells in copper maintained the most uniform heat pattern and displayed minimal temperature gradient challenges. Significant thermal differences occurring within the PVC case led to potential risks for both thermal degradation and

possible thermal runaway responses.

REFERENCES

[1] Shahid, S, Agelin-Chaab, M. (2017). Analysis of cooling effectiveness and temperature uniformity in a battery pack for cylindrical batteries. Energies, 10(8): 1157. https://doi.org/10.3390/en10081157

[2] Ma, S., Jiang, M.D., Tao, P., Song, C.Y., Wu, J.B., Wang, J., Deng, T., Shang, W. (2018). Temperature effect and thermal impact in lithium-ion batteries: A review. Progress in Natural Science: Materials International, 28(6): 653-666. https://doi.org/10.1016/j.pnsc.2018.11.002

[3] Senyshyn, A., Mühlbauer, M.J., Dolotko, O., Ehrenberg, H. (2015). Low-temperature performance of Li-ion batteries: The behavior of lithiated graphite. Journal of Power Sources, 282: 235-240. https://doi.org/10.1016/j.jpowsour.2015.02.008

[4] Jow, T.R., Delp, S.A., Allen, J.L., Jones, J.P., Smart, M.C. (2018). Factors limiting Li+ charge transfer kinetics in Li-Ion batteries. Journal of The Electrochemical Society, 165(2): A361. https://doi.org/10.1149/2.1221802jes

[5] Ghalkhani, M., Bahiraei, F., Nazri, G.A., Saif, M. (2017). Electrochemical–thermal model of pouch-type lithium-ion batteries. Electrochimca Acta, 247: 569-587. https://doi.org/10.1016/j.electacta.2017.06.164

[6] Ohsaki, T., Kishi, T., Kuboki, T., Takami, N., Shimura, N., Sato, Y., Sekino, M., Satoh, A. (2005). Overcharge reaction of lithium-ion batteries. Journal of Power Sources, 146(1-2): 97-100. https://doi.org/10.1016/j.jpowsour.2005.03.105

[7] Wang, Q.S., Ping, P., Zhao, X.J., Chu, G.Q., Sun, J.H., Chen, C.H. (2012). Thermal runaway caused fire and explosion of lithium ion battery. Journal of Power Sources, 208: 210-224. https://doi.org/10.1016/j.jpowsour.2012.02.038

[8] Dean, N. (2022). Mapping the electric car influencers. Nature Energy, 7(2): 121. https://doi.org/10.1038/s41560-022-00992-0

[9] Scott, S., Islam, Z., Allen, J., Yingnakorn, T., Alflakian, A., Hathaway, J., Rastegarpanah, A., Harper, G.D., Kendrick, E., Anderson, P.A. (2023). Designing lithium-ion batteries for recycle: The role of adhesives. Energy, 1(2): 100023. https://doi.org/10.1016/j.nxener.2023.100023

[10] Zhang, X., Chen, S., Zhu, J.Z., Gao, Y.Z. (2023). A critical review of thermal runaway prediction and early-warning methods for lithium-ion batteries. Energy Material Advances, 4: 0008. https://doi.org/10.34133/energymatadv.00

[11] Pagnanelli, F., Schiavi, P.G., Altimari, P. (2023). Direct recycling of lithium ion battery, what's next? Next Energy, 1(2): 100005. https://doi.org/10.1016/j.nxener.2023.100005

[12] Thakur, A.K., Sathyamurthy, R., Velraj, R., Saidur, R., Pandey, A., Ma, Z., Singh, P., Hazra, S.K., Sharshir, S.W., Prabakaran, R., Kim, S.C., Panchal, S., Ali, H.M. (2023). A state-of-the art review on advancing battery thermal management systems for fast-charging. Applied Thermal Engineering, 226: 120303. https://doi.org/10.1016/j.applthermaleng.2023.120303

[13] Youssef, R., Hosen, M.S., He, J.C., Jaguemont, J., Akbarzadeh, M., De Sutter, L., Van Mierlo, J., Berecibar, M. (2021). Experimental and numerical study on the thermal behavior of a large lithium-ion prismatic cell with natural air convection. IEEE Transactions on Industry Applications, 57(6): 6475-6482. https://doi.org/10.1109/TIA.2021.3108757

[14] Wilke, S., Schweitzer, B., Khateeb, S., Al-Hallaj, S. (2017). Preventing thermal runaway propagation in lithium ion battery packs using a phase change composite material: An experimental study. Journal of Power Sources, 340: 51-59. https://doi.org/10.1016/j.jpowsour.2016.11.018

[15] Väyrynen, A., Salminen, J. (2012). Lithium ion battery production. The Journal of Chemical Thermodynamics, 46: 80-85. https://doi.org/10.1016/j.jct.2011.09.005

[16] Wang, Z.W., Zhang, H.Y., Xia, X. (2017). Experimental investigation on the thermal behavior of cylindrical battery with composite paraffin and fin structure. International Journal of Heat and Mass Transfer, 109: 958-970. http://doi.org/10.1016/j.ijheatmasstransfer.2017.02.057

[17] Jiang, G.W., Huang, J.H., Liu, M.C., Cao, M. (2017). Experiment and simulation of thermal management for a tube-shell li-ion battery pack with composite phase change material. Applied Thermal Engineering, 120: 1-9. https://doi.org/10.1016/j.applthermaleng.2017.03.107

[18] Arora, S. (2018). Selection of thermal management system for modular battery packs of electric vehicles: A review of existing and emerging technologies. Journal of Power Sources, 400: 621-640. https://doi.org/10.1016/j.jpowsour.2018.08.020

[19] Yang, N.X., Zhang, X.W., Shang, B.B., Li, G.J. (2016). Unbalanced discharging and aging due to temperature differences among the cells in a lithium-ion battery pack with parallel combination. Journal of Power Sources, 306: 733-741. https://doi.org/10.1016/j.jpowsour.2015.12.079

[20] Yuan, W., Liang, D., Chu, Y.Y., Wang, Q.S. (2022). Aging effect delays overcharge-induced thermal runaway of lithium-ion batteries. Journal of Loss Prevention in the Process Industries, 79: 104830. https://doi.org/10.1016/j.jlp.2022.104830

[21] Shahjalal, M., Shams, T., Islam, M.E., Alam, W., Modak, M., Hossain, S.B., Ramadesigan, V., Ahmed, M.R., Ahmed, H., Iqbal, A. (2021). A review of thermal management for Li-ion batteries: Prospects, challenges, and issues. Journal of Energy Storage, 39: 102518. https://doi.org/10.1016/j.est.2021.102518

[22] Behi, H., Karimi, D., Behi, M., Ghanbarpour, M., Jaguemont, J., Sokkeh, M.A., Gandoman, F.H., Berecibar, M., van Mierlo, J. (2020). A new concept of thermal management system in Li-ion battery using air cooling and heat pipe for electric vehicles. Applied Thermal Engineering, 174: 115280. https://doi.org/10.1016/j.applthermaleng.2020.115280

[23] Yuen, A.C.Y., Chen, T.B.Y., Wang, C., Wei, W., Kabir, I., Vargas, J.B., Chan, Q.N., Kook, S., Yeoh, G.H. (2020). Utilising genetic algorithm to optimise pyrolysis kinetics for fire modelling and characterisation of chitosan/graphene oxide polyurethane composites. Composites Part B Engineering, 182: 107619. https://doi.org/10.1016/j.compositesb.2019.107619

[24] Sharma, A.R., Sai, C.S., Kumar, A., Reddy, R.V.J.,

Danyharsha, D., Jilte, R. (2021). Three-dimensional CFD study on heat dissipation in cylindrical lithium-ion battery module. Materials Today Proceedings, 46(9): 10964-10968. https://doi.org/10.1016/j.matpr.2021.02.041

[25] Yuen, A.C.Y., Yeoh, G.H. (2013). Numerical simulation of an enclosure fire in a large test hall. Computational Thermal Sciences an International Journal, 5(6): 459-471. https://doi.org/10.1615/ComputThermalScien.2013005954

[26] De Cachinho Cordeiro, I.M., Liu, H., Yuen, A.C.Y., Chen, T.B.Y., Li, A., Cao, R.F., Yeoh, G.H. (2022). Numerical investigation of expandable graphite suppression on metal-based fire. Heat and Mass Transfer, 58(1): 65-81. https://doi.org/10.1007/s00231-021-03097-8

[27] Li, W., Garg, A., Wang, N.B., Gao, L., le Phung, M.L., Tran, V.M. (2022). Computational fluid dynamics-based numerical analysis for studying the effect of mini-channel cooling plate, flow characteristics, and battery arrangement for cylindrical lithium-ion battery pack. Journal of Electrochemical Energy Conversion and Storage, 19(4): 041003. https://doi.org/10.1115/1.4054648

[28] Pansare, S.S., Patil, S.S. (2020). The mesh quality significance in finite element analysis. IOSR Journal of Mechanical and Civil Engineering, 17(2): 44-48. https://doi.org/10.9790/1684-1702054448

[29] Patil, S.S., Pansare, S.S. (2014). Meshing methodology for FEA analysis in ANSYS. International Journal for Scientific Research & Development, 2(3): 250-253. https://ijsrd.com/articles/IJSRDV2I3250.pdf.

[30] Mavi, A. (2023). Modelling and computational analysis of heat-transfer in multi-geometry and multi-phase flow of Newtonian and non-Newtonian fluids in pipes and channels. Master Thesis, Institutt for Energi og Prosessteknikk. https://hdl.handle.net/11250/3023112.

[31] Liu, M.Y., Jiang, C., Gao, G.J., Zhu, H.F., Xu, L. (2024). Assessment of RANS turbulence models based on the cell-based smoothed finite element model for prediction of turbulent flow. Engineering Analysis with Boundary Elements, 168: 105937. https://doi.org/10.1016/j.enganabound.2024.105937

[32] Lopez, C.F., Jeevarajan, J.A. (2015). Characterization of lithium-ion battery thermal abuse behavior using experimental and computational analysis. Journal of The Electrochemical Society, 162(10): A2163. https://doi.org/10.1149/2.0751510jes

[33] Feng, X.N., Ouyang, M.G., Liu, X., Lu, L.G., Xia, Y., He, X.M. (2018). Thermal runaway mechanism of lithium-ion battery for electric vehicles: A review. Energy Storage Materials, 10: 246-267. https://doi.org/10.1016/j.ensm.2017.05.013

[34] Gao, X., Chak, C., Hao, Q., Zeng, D., Xu, J. (2023). Thermal safety of lithium-ion batteries: Mechanism, modeling, and characterizations. Annual Reviews of Heat Transfer, 26(1). https://doi.org/10.1615/AnnualRevHeatTransfer.2023048695

[35] Alami, A.H., Maghrabie, H.M., Abdelkareem, M.A., Sayed, E.T., Yasser, Z., Salameh, T., Rahman, S.M.A., Rezk, H., Olabi, A.G. (2022). Potential applications of phase change materials for batteries' thermal management systems in electric vehicles. Journal of Energy Storage, 54: 105204. https://doi.org/10.1016/j.est.2022.105204

[36] Jamsawang, S., Chanthanumataporn, S., Sutthivirode, K., Thongtip, T. (2024). Investigation of the performance of battery thermal management based on direct refrigerant cooling: Simulation, validation of results, and parametric studies. Energies, 17(2): 543. https://doi.org/10.3390/en17020543